Research

Open Access

W Li, Q Huang *et al.*

The new therapeutic target of papillary thyroid carcinoma

700–707

6 : 700

RDM1 gene overexpression represents a therapeutic target in papillary thyroid carcinoma

Wei Li[1],*, **Qing Huang[2],***, **Danyang Sun[1]**, **Guizhi Zhang[1]** and **Jian Tan[1]**

[1]Department of Nuclear Medicine, Tianjin Medical University General Hospital, Tianjin, People's Republic of China
[2]Collage of Tourism and Service Management, Nankai University, Tianjin, People's Republic of China
*(W Li and Q Huang contributed equally to this work)

Correspondence should be addressed to W Li
Email
liwei01@tmu.edu.cn

Endocrine CONNECTIONS

Abstract

RAD52 motif containing 1 (*RDM1*) encodes the RAD52 protein involved in DNA double-strand break repair and recombination events. However, the importance of *RDM1* in papillary thyroid carcinoma (PTC) is largely unknown. In the present study, we examined the role of *RDM1* in thyroid cancer. The *RDM1* expression in PTC patients was examined using immunohistochemistry. The expression levels of *RDM1* mRNA in thyroid cancer cells were measured by quantitative real-time PCR (qRT-PCR). Lentivirus-mediated small interfering RNAs (siRNAs) were used to knock down the *RDM1* expression in the K1 and TPC1 cells. Then, changes in the *RDM1* target gene expression were determined by qRT-PCR and Western blot. Cell proliferation was examined by a high content screening assay. Cell cycle distribution and apoptosis were detected by flow cytometric analysis and MTT analysis. We showed that the *RDM1* expression was higher in PTC tissue compared to pericarcinous tissue. *RDM1* mRNA was found to be expressed by qRT-PCR. Using a lentivirus-based RNA interference (RNAi) approach, the *RDM1* expression was significantly inhibited. The inhibition of *RDM1* expression by RNAi significantly impaired cell proliferation, increased apoptosis and arrested cells in the G2/M phase. These data showed that *RDM1* was highly expressed in PTC tissue and thyroid cancer cell lines. Moreover, *RDM1* may play an important role in cell proliferation, cell cycle distribution and apoptosis of human PTC cells.

Introduction

Papillary thyroid carcinoma (PTC) is the most common subtype of thyroid cancer. In 2008, the incidence of thyroid cancer was 1.4/100,000, and it accounts for 0.8% of all malignancies in China (0.4% of those in men, 1.3% in women) (1). Through surgery and radioactive iodine ablation, most PTC patients have a good prognosis; however, a significant proportion of patients have persistent or recurrent disease and suffer from frequent recurrences or even distant metastases, leading to an unfavourable outcome. A minority of these patients will die from thyroid cancer (2).

The RAD52 motif containing 1 (*RDM1*) gene showed upregulation in PTC compared with normal thyroid tissues through an analysis of the gene expression dataset of Gene Expression Omnibus (GEO) and the Cancer Genome Atlas (TCGA). *RDM1* is located at 17q11.2 and belongs to the gene-binding motif containing family. *RDM1* contains a small amino acid motif, named the RD motif, which it shares with the recombination and repair protein RAD52 (3). *RDM1* can bind to RNA as well as single- and double-stranded DNA and is involved with DNA double-strand break (DSB) repair and recombination events. When the repair of DNA damage

occurs, many genes are involved in DNA repair, including excision repair, post-replication repair and recombination/DSB repair. The repair of DSBs is mediated extensively by RAD52-dependent recombination (4).

To explore the role of *RDM1* in PTC, an analysis of *RDM1* expression was conducted in thyroid cancer cell lines. Lentivirus-mediated small interfering RNA (siRNA) targeting of *RDM1* was used to downregulate gene expression. Then, experiments were performed to examine the effect of *RDM1* silencing on the cell cycle, apoptosis and proliferation.

Materials and methods

Patient clinical data

Before this study began, written informed consent was obtained from all patients who participated in the study, which was approved by the Ethics Committee of Tianjin Medical University General Hospital. A group of 23 PTC patients who underwent total thyroidectomy and neck lymph dissection in Tianjin Medical University General Hospital, China, was studied. Paraffin-embedded tissue material/tissue blocks were chosen for histological studies.

Analysis of gene expression database

To analyse comparative of *RDM1* expression, several web-based bioinformatics tools were used. GEO statistical tool (http://www.ncbi.nlm.nih.gov/geo/) and TCGA website (https://cancergenome.nih.gov/) were reciprocally employed (5). The microarray data were downloaded from website, relative gene expression and log2 fold change values of gene expression, and survival (Kaplan–Meier) curves were calculated, compared and statistically analysed through Excel and GEO2R, cBioPortal online tool (http://www.cbioportal.org/).

Cell lines

The human thyroid cancer cell lines K1 and TPC1 were used in our laboratory (6). All cell lines were cultured in Dulbecco's Modified Eagle Medium supplemented with 10% FBS and 1% penicillin/streptomycin. All culture reagents were purchased from Gibco. The cell cultures were stored in a humidified atmosphere containing 5% CO_2 buffered with ambient air at 37°C.

Immunohistochemical staining for *RDM1*

The specimens were immunostained using the PV-6000 immunohistochemistry method to evaluate the expression of the *RDM1* protein. The primary antibody used was *RDM1* rabbit polyclonal antibody (HPA024708, Sigma). The samples stained with *RDM1* antibodies were examined using a microscope (BX51, Olympus). The immunoreactivity of the samples was evaluated using a scoring scale that measured both the intensity and the percentage of cells positively stained. The staining intensity was scored as follows: 0 (none), 1 (weak), 2 (moderate) or 3 (intense). The percentage of positively stained cells was scored as follows: 0 (<1%), 1 (1–25%), 2 (25–50%), 3 (50–75%) or 4 (>75%). Immunoreactivity scores were then assigned according to the product of the two parameters evaluated (intensity and positivity) as follows: ≤6 was low expression and >6 was high expression (7).

Quantitative real-time PCR (qRT-PCR) for gene expression

Total RNA was extracted with TRIzol (Invitrogen) according to the manufacturer's instructions. One-step RT-PCR was carried out in triplicate with the following primers: *RDM1* (forward: 5′-GCCCATCCTGGTTTCTATGCCC-3′; reverse: 5′-AGACGAACCTTGACTGGAGAT-3′); GAPDH (forward: 5′-TGACTTCAACAGCGACACCCA-3; reverse: 5′-CACCCTGTTGCTGTAGCCAAA-3′). The *RDM1* gene expression was calculated using ΔCT and normalised to GAPDH. The relative gene expression after lentivirus infection was calculated using the $2^{-\Delta\Delta CT}$ method and normalised to GAPDH (8).

Lentivirus vectors for *RDM1* siRNA construction and transduction

Lentiviral vectors for *RDM1* siRNA were used to silence the *RDM1* gene expression. Lentivirus was used to express siRNAs targeting the *RDM1* sequence (Genbank No. NM_145654). The siRNA sequence was 5′-GGCCCATCCTGGTTTCTAT-3′. The sequences were cloned into pGCSIL (GeneChem, Shanghai, China) to generate the lentiviral vectors. *RDM1*-siRNA lentivirus is referred to as *shRDM1*; the negative control lentivirus that inserts a meaningless sequence (5′-TTCTCCGAACGTGTCACGT-3′) is referred to as shCtrl. shCtrl has no homology to any known human genes. K1 and TPC1 cells were infected with *shRDM1* and shCtrl,

Endocrine Connections

respectively. The interference efficiency of the template was detected by the Western blot analysis.

For lentivirus transduction, K1 and TPC1 cells were incubated with a 1:1 combination of culture medium and lentivirus medium. After 8 h of incubation, the medium was replaced with a complete culture medium, and the cells were allowed to grow for 3 days. The lentivirus-transduced cells were treated with 1 mg/mL puromycin for 48 h for stable clone selection (9).

Western blot analysis

The expression of the *RDM1* protein was studied in K1 and TPC1 cells by Western blotting as described earlier (10). Cells were harvested with a scraper after being washed with ice-cold phosphate-buffered saline and lysed in a buffer containing 10 mM Tris·HCl (pH 7.5), 1 mM DTT, 20% (v/v) glycerol, 1 mM ethylenediaminetetraacetic acid and a protease inhibitor mixture. Proteins were separated by SDS-PAGE, transferred onto PVDF membranes, stained with the primary antibodies *RDM1* rabbit-antibody (HPA024708, Sigma, 1:200) and GAPDH mouse-antibody (sc-32233, Santa-Cruz, 1:2000) at 4°C overnight and then incubated with secondary antibody at room temperature for 30 min. ECL Western blotting reagents were used for detection. Exposures were made at room temperature for 1–3 min using Fujifilm films. Prestained protein marker (26620, ThermoFisher) was run in the same gels to compare molecular weights and estimate transfer efficiency.

Flow cytometric analysis of cell cycle distribution and apoptosis

Flow cytometric analysis was performed to define the cell cycle distribution and induction of apoptosis in K1 and TPC1 cells. Values are an average of at least 3 independent experiments. Cells infected with *RDM1*-siRNA lentivirus were plated onto 6-well plates in triplicate and incubated at 37°C for 4 days. Cells were then collected, washed twice with ice-cold D-Hanks, fixed with 75% ice-cold ethanol, washed twice with ice-cold D-Hanks and stained with propidium iodide (PI, 2 mg/mL) in the presence of RNase (10 mg/mL). The cell cycle phase of K1 and TPC1 cells was analysed by flow cytometry. For induction of apoptosis, an Annexin V Apoptosis Detection Kit APC (eBioscience, USA) was used. Cells were plated and infected with *RDM1*-siRNA lentivirus as described earlier for the cell cycle assay. Following incubation at 37°C for 3 days, cells were collected and stained with 10 μL of Annexin V-APC away from light. The percentage of apoptotic cells was identified.

Plate analysis with the adherent cell cytometry system Celigo

K1 and TPC1 cells were analysed with fluorescence staining after lentivirus transduction to quantify the cellular siRNA gene knockdown rate. The adherent cell cytometry system allowed rapid quantification of cellular fluorescence as previously described (11). 96-Well plates were analysed using an adherent cell cytometer equipped with bright field and green filter fluorescent channels. Gating parameters were adjusted for the fluorescence channel to exclude background and other non-specific signals. The Celigo system provided a gross quantitative analysis for each fluorescence channel and individual well, including the total count and the average integrated red fluorescence intensity of gated events.

MTT cell viability assay

The inhibition of cell proliferation following treatment with the extract was measured using an MTT assay. Briefly, K1 and TPC1 cells infected with *shRDM1* or shCtrl were separately plated in 96-well plates (2000 cells/well). Following 1–5 days of incubation at 37°C, 20 μL of MTT solution (5 mg/mL) was added to the cells, and then the cells were incubated for 4 h. Then, the supernatant was removed, 150 μL of DMSO was added, and then the samples were shaken for 5 min until the crystal dissolved. The absorbance was measured using a microplate reader (Infinite 200 PRO series; TECAN) at a wavelength of 490 nm. The optical density (OD) value at 490 nm was measured by an enzyme-linked immunosorbent assay reader. The negative control well had no cells and was used as the zero point of absorbance. All the experiments in each group were performed in triplicate (12).

Statistical analysis

Data were expressed as the mean ± S.D. Comparison between two groups and two or more independent groups was done with independent sample *T*-test, and one-way ANOVA. $P < 0.05$ indicates significant difference.

Results

RDM1 is upregulated in PTC

Using the GEO data mining platform, we performed a comprehensive analysis of *RDM1* expression profiles in various types of thyroid cancer vs normal thyroid tissues

(a total of 21 clinical samples including PTC, the follicular variant of papillary thyroid carcinoma (FVPTC), poorly differentiated thyroid carcinoma (PDTC) and normal thyroid tissue) that was reported in a previous study (13). The data showed no statistical significance, because normal thyroid tissue had only one patient (Fig. 1A). Then, we performed a comprehensive analysis of *RDM1* expression profiles in various types of thyroid cancer vs normal thyroid tissues (a total of 105 clinical samples including papillary, anaplastic thyroid cancer and patients with no-tumour control) that was reported in a previous study (14). This analysis described that PTC showed a consistent upregulation of *RDM1* compared to normal thyroid tissues, and the relative gene expression of *RDM1* in PTC was about 1.2-fold higher than normal thyroid tissue (Fig. 1B). Moreover, we also performed a comprehensive analysis

of *RDM1* expression in different PTC tissues (compared with PTC primary lesion, lymph node metastasis, normal lymph node and recurrent tumour at N0 and N1 stages); the result described an upregulation *RDM1* expression of primary lesion and lymph node at N1 stage patients (Fig. 1D) than primary lesion of N0 stage. But compared with different tumour T stages (T1 or T2 vs T2 or T3), the data showed no statistical significance (Fig. 1C).

The *RDM1* expression of thyroid tumour and normal thyroid tissue (a total of 568 clinical samples, include 58 normal thyroid tissue and 508 PTC) was analysed using the RNAseqV2 datasets for thyroid cancer deposited on TCGA (https://cancergenome.nih.gov/) website (5). The data indicated that the *RDM1* expression was increased by more than 2-fold (Fig. 1E). Based on TCGA data, we used cBioPortal (http://www.cbioportal.org) to draw
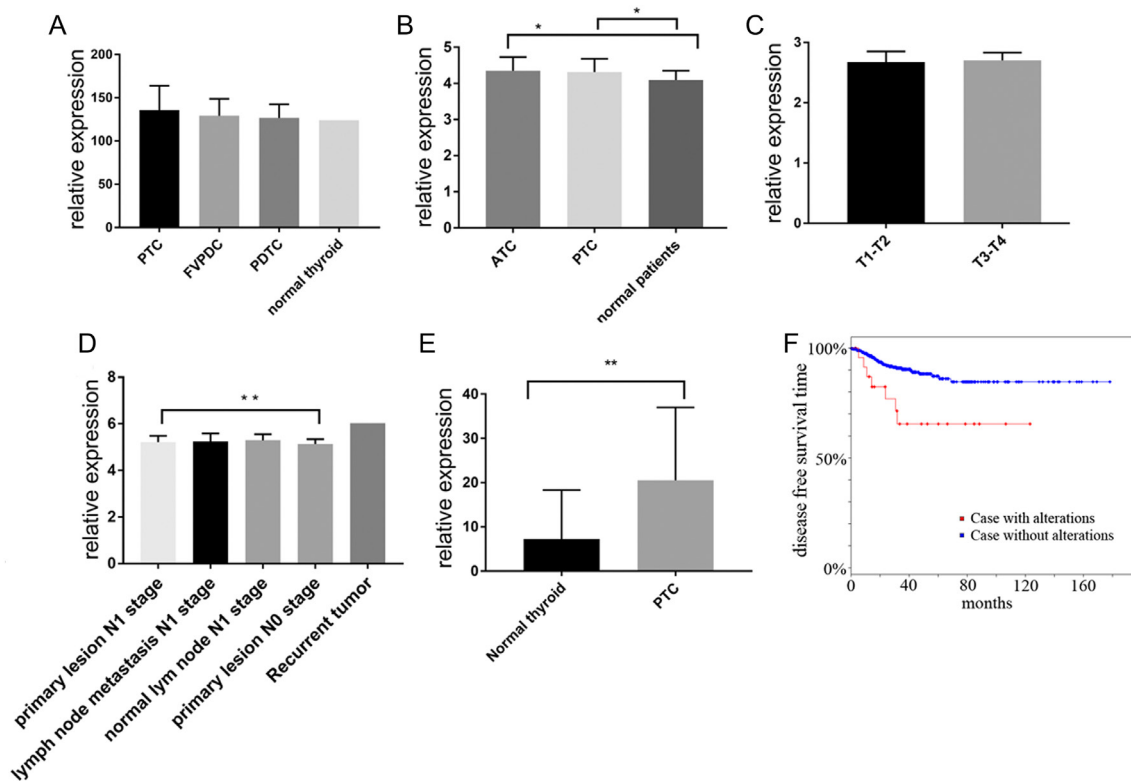

Figure 1

RDM1 expression in thyroid cancer from the GEO and TCGA datasets. (A) *RDM1* expression in PTC, FVPTC, PDTC and normal thyroid tissue (PTC, $n=7$; FVPTC, $n=8$; PDTC, $n=5$; normal thyroid tissue, $n=1$). Data source: GSE53157. PTC=135.8±28.18, FVPTC=129.2±6.91, PDTC=126.8±6.99, normal thyroid tissue=123.9. $P=0.88$. (B) *RDM1* expression in ATC, PTC and normal patients' thyroid (ATC, $n=11$; PTC, $n=49$; normal patients' thyroid, $n=45$). Data source: GSE33630. ATC=4.35±0.38, PTC=4.31±0.37, normal thyroid=4.09±0.26. *$P<0.05$. (C) *RDM1* expression in T1–T2 and T3–T4 PTC patients (T1–T2, $n=21$; T3–T4, $n=15$). Data source: GSE65074. T1–T2=2.68±0.04; T3–T4=2.71±0.03. $P=0.57$. (D) *RDM1* expression in PTC primary lesion, lymph node metastasis, normal lymph node and recurrent tumour at N0 and N1 stages. Primary lesion N1 stage, $n=20$; primary lesion N0 stage, $n=14$; lymph node metastasis N1 stage, $n=21$; normal lymph node N1 stage, $n=4$; Recurrent tumour, $n=1$. Data source: GSE60542. Primary lesion N1 stage=5.21±0.28; primary lesion N0 stage=5.14±0.21; lymph node metastasis N1 stage=5.24±0.35; normal lymph node N1 stage=5.29±0.26; Recurrent tumour=6.02. **$P<0.01$. (E) *RDM1* expression in 568 pairs of PTCs and normal thyroid tissue from TCGA RNA-seq data (normal thyroid, $n=58$; PTC, $n=510$). PTC=20.51±0.73; normal thyroid=7.26±1.45. **$P<0.01$. (F) Disease-free survival (Kaplan–Meier) curves. Cases with alteration (mRNA expression z-scores choose >2 or <−2) were 24 (relapsed $n=7$, 29.17%), without alteration were 469 (relapsed $n=41$, 8.74%).

disease-free survival (Kaplan–Meier) curves and genomic profiles condition: mRNA expression *z*-scores choose >2 or <−2. Kaplan–Meier curves for the survival of patients with the *RDM1* expression being changed more than 2-fold were significantly lower than control (logrank test *P*-value: 0.00321). Survival probabilities (95% confidence intervals) at 40, 80 and 120 months are as follows: for 89.67% vs 65.45%, 84.61% vs 65.45% and 84.61% vs 65.45%, respectively (Fig. 1F).

To further validate the expression of *RDM1* in thyroid cancer, we used immunoreactivity scores to examine the *RDM1* expression in the tumours and pericarcinous tissue (the same patient's normal thyroid tissues) of 23 pairs PTC patients. The immunoreactivity scores of *RDM1* positive percentage were significantly higher in the tumours than in the pericarcinous tissue (immunoreactivity scores: 2.2 ± 0.4, 0.2 ± 0.1, $P<0.01$) (Fig. 2C). In agreement with the TCGA data, the *RDM1* expression was higher in most thyroid tumour tissues in comparison with their pericarcinous tissue. Examples of typical immunostaining of positive and negative *RDM1* expressions are presented in Fig. 2A and B.

The clinical characteristics of 23 PTC patients were as follows. The patients consisted of 2 males and 21 females. The ages of the patients were from 47 to 76 years old, with an average age of 55.5 ± 7.6 years. One patient had a bilateral tumour, and 22 patients had unilateral tumours. Extrathyroidal extension occurred in 17 patients. Twenty-two patients presented with lymph node metastases and none reported distant metastasis. Three patients were diagnosed with Hashimoto thyroiditis by pathological examination.

The *RDM1* expression is downregulated by *shRDM1* in K1 and TPC1 cells

After 8h of infection with *shRDM1* or shCtrl, the thyroid cancer cells were incubated for 72h and then observed with a fluorescence microscope. The infection efficiency was more than 80% and the cells remained healthy.

The *RDM1* mRNA expression level in K1 and TPC1 cells was high when normalised to the GAPDH expression, as analysed by qRT-PCR (Fig. 3A). K1 and TPC1 cells were infected with either *shRDM1* or shCtrl lentivirus. The *RDM1* protein level detected by Western blot was reduced in *RDM1*-siRNA infected cells, indicating effective knockdown of the target sequence (Fig. 3B). Compared with cells infected with control lentivirus shCtrl, the *RDM1* mRNA expression in cells infected with *shRDM1* was lower ($P<0.01$). The knockdown efficiency of *shRDM1* was about 51% and 70% in K1 and TPC1 cells, respectively, as determined by qRT-PCR (Fig. 3C and D). The results indicated that the interference efficiency was valid in K1 and TPC1 cells.

Knockdown of *RDM1* expression by RNA interference (RNAi) induces apoptosis and G2/M arrest

In addition, to determine whether *RDM1*-siRNA enhanced cell apoptosis by the induction of cell cycle arrest, K1 and TPC1 cells were infected with lentivirus and incubated for 3–4 days, and then the cell cycle distribution and apoptosis were evaluated by the flow cytometric analysis. As shown in Fig. 4A and C, the inhibited expression of *RDM1* resulted in an increase in the apoptosis of K1 and TPC1 cells. The cell cycle analysis showed an increased percentage of cells in the G2/M phase ($P<0.01$) in K1 and TPC1 cells and a decreased population in G1 phase ($P<0.01$) in K1 cells (Fig. 4B, C and D). The population showed no significant difference in the S phase.

The ability of cell proliferation was significantly inhibited by cell count analysis and MTT

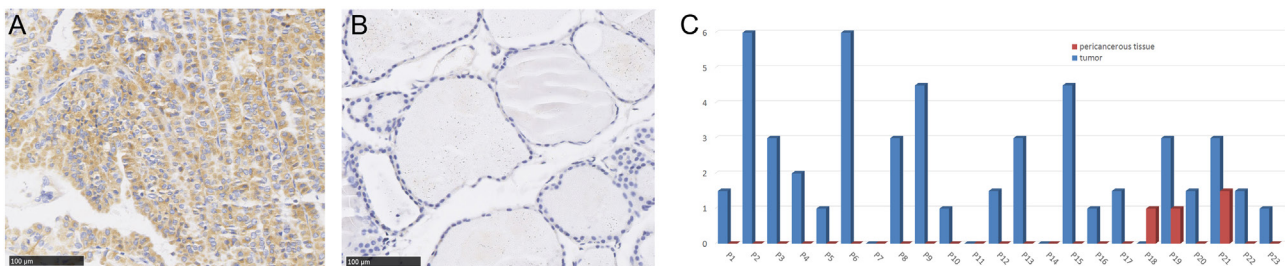Celigo software was used to generate representative scatter plots that depict the green fluorescence area

Figure 2

RDM1 expression in the immunohistochemical analysis. (A) Typical immunohistochemistry staining of *RDM1* positive in PTC tissue (×40). (B) Typical immunohistochemistry staining of *RDM1* negative in pericarcinous tissue/normal thyroid tissue (×40). (C) Expression of *RDM1* in 23 paired PTCs and pericarcinous tissue by the immunoreactivity score analysis.
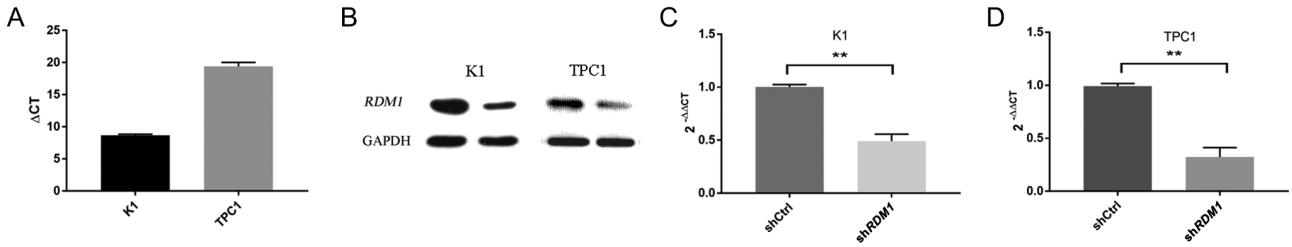
Figure 3
RDM1 expression examined by qRT-PCR and Western blot. CT is the threshold cycle for target amplification in K1 cells. ΔCT is equal to the difference in threshold cycles for the target and reference; ΔΔCT calculates the relative quantification of target. (A) *RDM1* mRNA expression level in K1 and TPC1 cells. ΔCT = CT$_{RDM1}$ − CT$_{GAPDH}$. (B) *RDM1* protein in K1and TPC1 cells. Compared with shCtrl, the level of *RDM1* protein in K1 and TPC cells decreased after the *RDM1* expression was silenced by RNAi. GAPDH is a control. The *RDM1* and GAPDH proteins were observed as major bands corresponding to molecular weights of 26 and 34 kDa, respectively. (C) and (D) Knock down efficiency was determined by qRT-PCR. The *RDM1* mRNA expression level in K1 cells after infection with different lentiviruses was measured using the 2$^{-ΔΔCT}$ method. ΔΔCT = mean (CT$_{RDM1}$/CT$_{GAPDH}$) − CT$_{RDM1}$. 2$^{-ΔΔCT}$ of *shRDM1* and shCtrl in K1 and TPC1 cells were 0.5 ± 0.1 vs 1.0 ± 0.0, 0.3 ± 0.1 vs 0.9 ± 0.0, respectively (**P < 0.01).

(in μm^2) and integrated fluorescence intensity (sum of the pixel intensities within a gated event) of the gated events in the individual treatment groups (11, 15). Strong differences in total count were observed between cells infected with *shRDM1* and shCtrl. From 1 day to 5 days, the fluorescence pixel counts/cell in K1 and TPC1 cells

infected with *shRDM1* were significantly lower than those in cells transfected with shCtrl (Fig. 5A and B). The K1 and TPC1 cell growths were significantly inhibited by *RDM1*-siRNA.

The cell density OD 490 was measured to calculate cell growth by the MTT analysis. As shown in Fig. 5C and D,
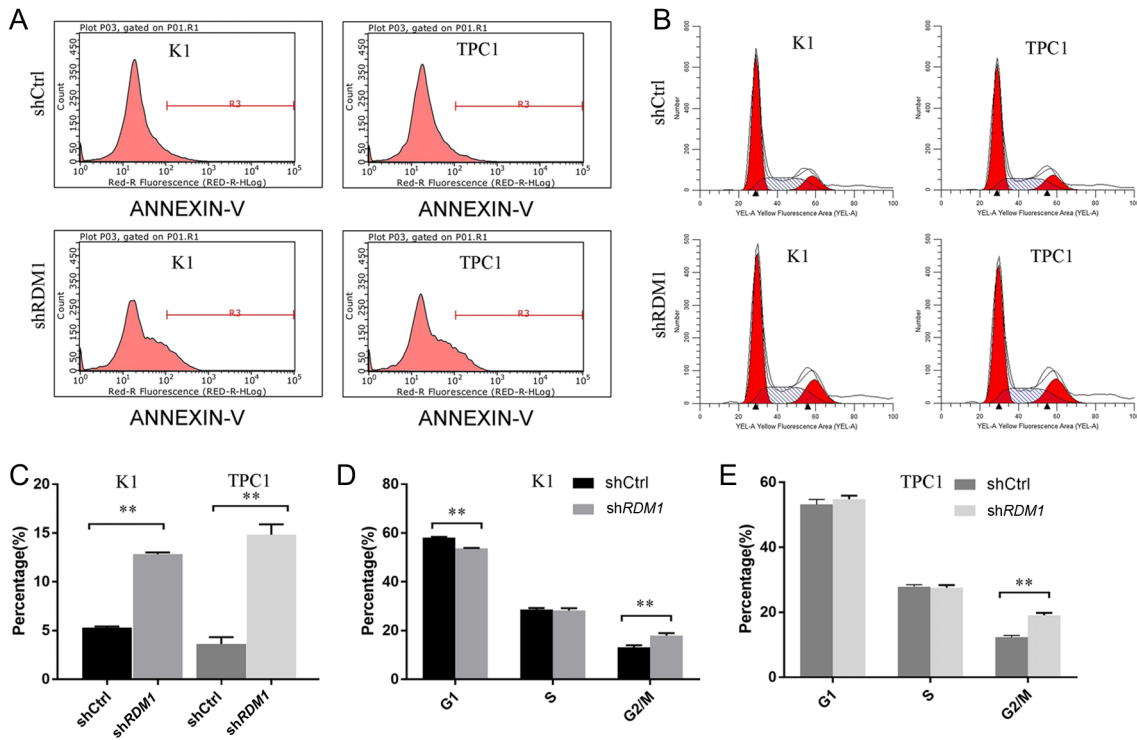

Figure 4
Effect of the downregulation of *RDM1* on K1 cells. (A) and (C) *RDM1*-siRNA enhanced cell apoptosis (*n* = 3). Flow cytometry analyses of apoptosis were shown in *shRDM1* and control vector in K1 and TPC1 cells. The apoptosis rate was observed to be 5.3 ± 0.1% (shCtrl) and 12.8 ± 0.2% (*shRDM1*) in K1 cells. The apoptosis rate was observed to be 3.6 ± 0.7% (shCtrl) and 14.8 ± 1.1% (*shRDM1*) in TPC1 cells. **P < 0.01, compared with shCtrl. (B), (C) and (E) *RDM1* expression affects cell cycle distribution (*n* = 3). The cell cycle analyses of *shRDM1* and control vector in K1 cells were 18.0 ± 1.0% and 13.2 ± 0.8% in the G2/M phase, and 58.2 ± 0.3% and 53.8 ± 0.2% in the G1/S phase. The cell cycle analyses of *shRDM1* and control vector in TPC1 cells were 19.1 ± 0.7% and 12.3 ± 0.5% in the G2/M phase, and 54.8 ± 1.1% and 53.2 ± 1.6% in the G1/S phase. **P < 0.01, compared with shCtrl.

the proliferation inhibition of *RDM1*-siRNA in K1 and TPC1 cells was time-dependent: it was noticeable on day 5.

Discussion

RDM1 encodes a 284-amino-acid-long protein and binds RNA, ssDNA and dsDNA. *RDM1* can increase sensitivity of chemotherapy drug cisplatin and may have a possible role during spermatogenesis and in the maintenance of stemness (3, 16). The mechanism of *RDM1* increases sensitivity of cisplatin such that the RD motif of *RDM1* plays a role in the interaction of the protein with nucleic acids, possibly as a modulator of the RRM, and/or that it is involved in the ability of *RDM1* to self-interact, as illustrated in this study by the filament-like structures observed on dsDNA (16). In 2007, a study showed that *RDM1* has a function in the heat-shock response (8).

Currently, there are few studies of *RDM1*. *RDM1* expression and function in thyroid cancer had not been studied. Thus, this study first explored the expression levels of *RDM1* in thyroid cancer tissue and thyroid cancer cell lines and found that it was more expressed in thyroid cancer tissue compared with pericancerous tissue. The expression of *RDM1* was also analysed at both the gene and miRNA levels in a large dataset of tumour and normal samples obtained from TCGA and GEO. As discussed in detail in the Results section, the high expression of *RDM1* was also confirmed at our immunohistochemistry samples. To assess the *RDM1* effect in thyroid cancer cell lines, these cells were

infected with *RDM1*-siRNA lentivirus or control lentivirus. Compared to the controls, *RDM1*-siRNA-treated cells showed decreased proliferation, increased apoptosis and an increase in the proportion of cells in the G2/M phases. Therefore, *RDM1* may promote thyroid cancer cell growth. To further clarify the mechanism of *RDM1*-siRNA growth inhibition, its ability to arrest cell cycle has been studied. The data suggest that *RDM1*-siRNA has the ability to arrest the cell cycle in the G2/M phase. Cell cycle progression and cell division are driven by the sequential activation of a group of serine–threonine kinases called cyclin-dependent kinases (CDKs). The activity of CDKs is positively regulated by cyclins and is negatively regulated by CDK inhibitors. The G2/M transition is regulated by the sequential activation and deactivation of CDK-regulatory proteins and cyclin complexes Moreover, DNA DSB repair is known to proceed via two major mechanisms: homologous recombination (HR) and non-homologous end joining. HR includes the exchange of genetic information between homologous or homoeologous DNA sequences and is thus generally active in the S and G2 phases of the cell cycle (17, 18). RD motif is the RRM domain of *RDM1* conserved in the DNA recombination and repair protein Radiation sensitive 52 (RAD52). RAD52 is an important HR protein (19). Experiments have shown that when recombinational repair is absent, hRAD52 expresses very low levels during the G1 phase, but through homologous repair rising, its level rises steadily through the S phase, reaching a maximum in the G2 phase (20). However, why *RDM1*-siRNA influences the G2/M phase and how *RDM1* plays a role in thyroid cancer are currently unknown and warrant further study.
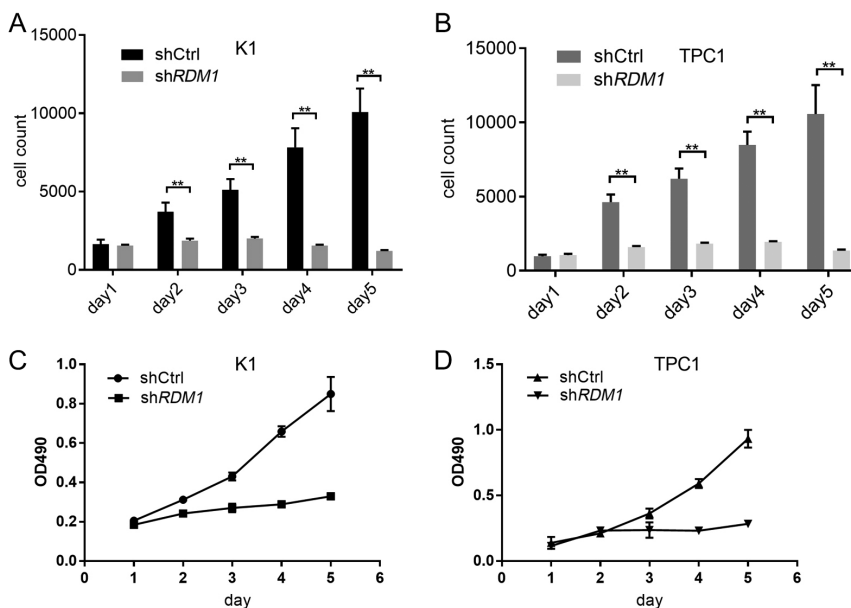

Figure 5

Growth analysis of K1 and TPC1 cells after infected with lentivirus (*n*=3). The proliferation of K1 and TPC1 cells was inhibited slightly by *RDM1*-siRNA, and analysed by Celigo cytometer and MTT. (A) and (B) Cell growth rate using Celigo cytometer. Cell growth rate was defined as the cell count of Nth day/cell count of 1st day. K1 and TPC1 cells infected shCtrl grew quickly; however, those cells infected *shRDM1* which showed growth retardation. **$P < 0.01$. (C) and (D) Growth curves by MTT. The K1 cell density OD 490 in the presence of *RDM1*-siRNA and in the control group were 0.24 ± 0.01 and 0.31 ± 0.00, respectively, on day 2; 0.33 ± 0.01 and 0.85 ± 0.09, respectively, on day 5. The TPC1 cell density compared with *shRDM1* and shCtrl were 0.21 ± 0.00 and 0.23 ± 0.01, respectively, on day 2; 0.29 ± 0.03 and 0.93 ± 0.07, respectively, on day 5.

Conclusion

This study highlights critical roles for *RDM1* in the PTC cell line. The data may provide the basis for further exploration of the role of *RDM1* in the occurrence and development of thyroid cancer. A follow-up study on the mechanism by which *RDM1* affects PTC cell biology is needed. *RDM1* may become a new target of PTC molecular therapy.

References

1 Chen W, Zheng R, Baade PD, Zhang S, Zeng H, Bray F, Jemal A, Yu XQ & He J. Cancer statistics in China, 2015. *CA: A Cancer Journal for Clinicians* 2016 **66** 115–132. (doi:10.3322/caac.21338)

2 Duman BB, Kara OI, Uguz A & Ates BT. Evaluation of PTEN, PI3K, MTOR, and KRAS expression and their clinical and prognostic relevance to differentiated thyroid carcinoma. *Contemporary Oncology* 2014 **18** 234–240. (doi:10.5114/wo.2014.43803)

3 Hamimes S, Bourgeon D, Stasiak AZ, Stasiak A & Van Dyck E. Nucleic acid-binding properties of the RRM-containing protein RDM1. *Biochemical and Biophysical Research Communications* 2006 **344** 87–94. (doi:10.1016/j.bbrc.2006.03.154)

4 Milne GT, Ho T & Weaver DT. Modulation of Saccharomyces cerevisiae DNA double-strand break repair by SRS2 and RAD51. *Genetics* 1995 **139** 1189–1199.

5 Liang W, Guan H, He X, Ke W, Xu L, Liu L, Xiao H & Li Y. Down-regulation of SOSTDC1 promotes thyroid cancer cell proliferation via regulating cyclin A2 and cyclin E2. *Oncotarget* 2015 **6** 31780–31791. (doi:10.18632/oncotarget.5566)

6 Tanaka J, Ogura T, Sato H & Hatano M. Establishment and biological characterization of an in vitro human cytomegalovirus latency model. *Virology* 1987 **161** 62–72. (doi:10.1016/0042-6822(87)90171-1)

7 Wei XL, Wang DS, Xi SY, Wu WJ, Chen DL, Zeng ZL, Wang RY, Huang YX, Jin Y, Wang F, *et al*. Clinicopathologic and prognostic relevance of ARID1A protein loss in colorectal cancer. *World Journal of Gastroenterology* 2014 **20** 18404–18412. (doi:10.3748/wjg.v20.i48.18404)

8 Messaoudi L, Yang YG, Kinomura A, Stavreva DA, Yan G, Bortolin-Cavaille ML, Arakawa H, Buerstedde JM, Hainaut P, Cavaille J, *et al*. Subcellular distribution of human RDM1 protein isoforms and their nucleolar accumulation in response to heat shock and proteotoxic stress. *Nucleic Acids Research* 2007 **35** 6571–6587. (doi:10.1093/nar/gkm753)

9 Wang Z, Xie Q, Yu Z, Zhou H, Huang Y, Bi X, Wang Y, Shi W, Sun H, Gu P, *et al*. A regulatory loop containing miR-26a, GSK3beta and C/EBPalpha regulates the osteogenesis of human adipose-derived mesenchymal stem cells. *Scientific Reports* 2015 **5** 15280. (doi:10.1038/srep15280)

10 Sasaki T, Lorkovic ZJ, Liang SC, Matzke AJ & Matzke M. The ability to form homodimers is essential for RDM1 to function in RNA-directed DNA methylation. *PLoS ONE* 2014 **9** e88190. (doi:10.1371/journal.pone.0088190)

11 Nabzdyk CS, Chun M, Pradhan L & Logerfo FW. High throughput RNAi assay optimization using adherent cell cytometry. *Journal of Translational Medicine* 2011 **9** 48. (doi:10.1186/1479-5876-9-48)

12 Wu GS, Zou SQ, Liu ZR, Tang ZH & Wang JH. Celecoxib inhibits proliferation and induces apoptosis via prostaglandin E2 pathway in human cholangiocarcinoma cell lines. *World Journal of Gastroenterology* 2003 **9** 1302–1306. (doi:10.3748/wjg.v9.i6.1302)

13 Pita JM, Banito A, Cavaco BM & Leite V. Gene expression profiling associated with the progression to poorly differentiated thyroid carcinomas. *British Journal of Cancer* 2009 **101** 1782–1791. (doi:10.1038/sj.bjc.6605340)

14 Tomás G, Tarabichi M, Gacquer D, Hébrant A, Dom G, Dumont JE, Keutgen X, Fahey TJ 3rd, Maenhaut C & Detours V. A general method to derive robust organ-specific gene expression-based. *Oncogene* 2012 **31** 4490–4498. (doi:10.1038/onc.2011.626)

15 Nabzdyk CS, Chun M, Pradhan Nabzdyk L, Yoshida S & LoGerfo FW. Differential susceptibility of human primary aortic and coronary artery vascular cells to RNA interference. *Biochemical and Biophysical Research Communications* 2012 **425** 261–265. (doi:10.1016/j.bbrc.2012.07.078)

16 Hamimes S, Arakawa H, Stasiak AZ, Kierzek AM, Hirano S, Yang YG, Takata M, Stasiak A, Buerstedde JM & Van Dyck E. RDM1, a novel RNA recognition motif (RRM)-containing protein involved in the cell response to cisplatin in vertebrates. *Journal of Biological Chemistry* 2005 **280** 9225–9235. (doi:10.1074/jbc.M412874200)

17 Barlow JH & Rothstein R. Timing is everything: cell cycle control of Rad52. *Cell Division* 2010 **5** 7. (doi:10.1186/1747-1028-5-7)

18 Li X & Heyer WD. Homologous recombination in DNA repair and DNA damage tolerance. *Cell Research* 2008 **18** 99–113. (doi:10.1038/cr.2008.1)

19 Game JC & Mortimer RK. A genetic study of X-ray sensitive mutants in yeast. *Mutation Research* 1974 **24** 281–292. (doi:10.1016/0027-5107(74)90176-6)

20 Chen F, Nastasi A, Shen Z, Brenneman M, Crissman H & Chen DJ. Cell cycle-dependent protein expression of mammalian homologs of yeast DNA double-strand break repair genes Rad51 and Rad52. *Mutation Research* 1997 **384** 205–211. (doi:10.1016/S0921-8777(97)00020-7)

Endocrine Connections